



VI Congreso Iberoamericano de Acústica - FIA 2008
Buenos Aires, 5, 6 y 7 de noviembre de 2008

FIA2008-xxx

Acoustic scattering from superspheroidal objects

Christopher Feuillade

Laboratorio de Acústica, Universidad Tecnológica de Chile-INACAP, Sede Pérez Rosales, Brown Norte 290, Ñuñoa 779-0569, Santiago, Chile. E-mail: chris.feuillede@gmail.com

Abstract

A T-matrix technique has been used to study acoustic scattering from extended axisymmetric objects. The objects are formed using the mathematical function for a “superellipse” [i.e. $(x/a)^s + (z/b)^s = 1$, where $s=2n$, $n=1,2,3,\dots$], and revolving around the z -axis. For $s=2$, the object is a spheroid with aspect ratio $\alpha=b/a$. As s increases, the shape of the object approaches a cylinder of radius a and length $2b$. The method allows the scattered field to be determined for all azimuth angles as a function of frequency, and allows comparisons to be made with other methods for describing the scattering of objects of this type. The results have direct applications in the interpretation of acoustic scattering from oceanic objects such as the swim bladders of some fish, and zooplankton.

Resumen

Una técnica de la extensión de la matriz-T se ha utilizado para estudiar la dispersión acústica de objetos axisimétricos alargados. Los objetos son formados a partir de la función matemática de una “super” elipse “ [i.e. $(x/a)^s + (z/b)^s = 1$, donde $s=2n$, $n=1,2,3,\dots$], y girando alrededor del eje z . Para $s=2$, el objeto es un esferoide alargado con razón de aspecto $\alpha=b/a$. A medida que s aumenta, el objeto se aproxima más a un cilindro con radio a y longitud $2b$. El método permite determinar la distribución del campo dispersado para todos los ángulos azimutales como una función de la frecuencia, y permite hacer comparaciones con otros métodos aproximados para describir la dispersión de objetos de este tipo. Los resultados tienen aplicaciones directas en la interpretación de la dispersión acústica de objetos oceánicos tales como las vejigas natatorias de algunos peces y en el zooplancton.

1 Introduction

Air bubbles in water have remarkable acoustical properties. The great difference between the acoustic impedances of air and water causes them to be highly effective scatterers of sound, especially when insonified at the primary (monopole) resonance frequency, where the bubble surface moves in and out without change in shape). In this case, the scattering cross-section may be many times larger than the physical bubble size. A classical introduction to the phenomena of bubbles is given in "Physics of Sound in the Sea" (1969).

The acoustic response of a spherical bubble was first treated by Minnaert (1933), using an equation of motion method he was able to predict the monopole resonance frequency as

$$ka = \frac{1}{c} \sqrt{\frac{3\gamma P}{\rho}}, \quad (1)$$

where: $k = 2\pi/\lambda$ is the wave number at the resonance frequency; a is the bubble radius; γ is the ratio of gas specific heats; and P , ρ , and c , are the ambient pressure, density, and sound speed, respectively, of the surrounding water. For an air bubble at atmospheric pressure in water ($c \approx 1500$ m/s) the value of $ka \approx 0.0136$. This means that the wavelength of sound at the monopole resonance frequency of the bubble is about 460 times its radius.

An alternative method of studying the acoustic resonances of a bubble is to examine sound scattering from its surface. In Anderson's (1950) fluid sphere theory, a bubble is characterized as a spherical void filled with air placed within the larger mass of water. This method predicts a monopole resonance frequency identical to that obtained by Minnaert.

An important research area for both bubbles and fish swimbladders (which behave very similarly to air bubbles) is their resonance behaviour in nonspherical cases. This was studied initially by Strasberg (1953) and Weston (1967), who examined the variation in the monopole resonance frequency for both oblate and prolate spheroidal cases, and found approximate values for the variable scattering cross-section, and Q. Ye (1998) also described sound scattering by a prolate spheroidal bubble, using an approach based on the Kirchhoff integral theorem, and an analogy between resonant scattering and electrostatic field phenomena.

In previous work (Feuillade and Werby, 1994), scattering from deformed bubbles was studied, using the extended boundary condition (EBC) method of Waterman (1969), (sometimes called the "T"-matrix method). In the spherical limit this is equivalent to Anderson's theory. Prolate spheroids, and cylinders with hemispherical endcaps, were considered. Variations in the resonance frequency, scattering amplitude, and Q, were studied; and the azimuthal scattering distribution.

Another approach to the swimbladder scattering problem has centered on the application of finite length fluid-filled cylinder and bent cylinder approximations (Stanton, 1988, 1989) for modeling the bladder.

In this present work, the EBC method is extended to consider low frequency scattering from air-filled objects in water, modelled as prolate "superspheroids." A superspheroid is a three-dimensional surface described in cartesian coordinates by the "superellipse" equation

$$\left(\frac{x}{a}\right)^s + \left(\frac{z}{b}\right)^s = 1 \quad (s = 2n, n = 1, 2, \dots), \quad (2)$$

which is revolved around the z axis to produce an axially symmetric object described by $\left(x/a\right)^s + \left(y/a\right)^s + \left(z/b\right)^s = 1$. Here, a is the semi-minor axis in the x and y directions, and b is the semi-minor axis in the z direction. The surface has aspect ratio $\alpha = b/a$. If $\alpha > 1$, it is

prolate, and if $\alpha < 1$, it is oblate. The exponent s describes the order of the superspheroid. If $s=2$, it is a regular spheroid; while, if $s > 2$, the surface changes such that, as s increases, the shape approaches that of a right circular cylinder of length $2b$, and radius a , with its axis in the z direction.

The purpose of the present work is to study the primary resonance scattering frequency, and distribution, of highly deformed bubbles for large values of s , since this method offers the capability of describing these phenomena for objects which closely approximate an exact right circular cylinder. Swimbladders are irregularly shaped objects, and typically only roughly resemble prolate spheroids, cylinders with hemispherical endcaps, or right circular cylinders. However, the presence of rough irregularities on the surface of the swimbladder is frequently assumed to cause only minor, and generally negligible, perturbations to the resonance frequency and scattering distribution of the swimbladder, which is dominated overall by the monopole resonance, and can be modelled using prolate spheroidal or cylindrical models. The work presented here makes a contribution to this topic, by examining the variation of these phenomena as the shape of the objects are successively deformed from a prolate spheroidal shape into a right circular cylinder of the same volume, which thereby introduces a sharp irregularity onto the contour of the surface. The results show that the assumption that the effect of surface irregularities is generally negligible appears to be well justified, and that the monopole resonance, which leads to a spherically symmetric scattering distribution, continues to dominate low frequency scattering even for cylindrically shaped, air-filled, objects with aspect ratios as high as $\alpha = 40$.

2 Theory

2.1 The EBC method

A complete development of the EBC method will not be presented here. For the derivation of the EBC theorem, the reader is referred to Waterman's original paper. A brief summary of the T-matrix expansion for a superspheroidal scatterer is given here.

In order to expand the T-matrix, the various components of the acoustic field (the incident, scattered, and internal, components) must be expanded in terms of a set of basis functions which are partial wave solutions of the Helmholtz equation, i.e.,

$$\{\nabla^2 + k^2\} \phi(\mathbf{r}) = 0, \quad (3)$$

with the center of the coordinate system placed inside the scatterer S . These solutions, which, for the scattering geometries considered here, are typically products of spherical Bessel (or spherical Hankel) functions with spherical harmonics, are denoted as $\{\psi_n(\mathbf{r}); n = 0, 1, 2, \dots\}$, where various indices have been condensed into n for simplicity, and \mathbf{r} is the field expansion point. The incident wave must have no singularities at the origin, so it is expanded using the regular wavefunctions $\{\text{Re}\psi_n(\mathbf{r})\}$ (involving products with spherical Bessel functions), i.e.,

$$\phi_o(\mathbf{r}) = \sum_n a_n \text{Re}\psi_n(\mathbf{r}). \quad (4)$$

The incident field is assumed to have no singularities inside the scattering surface S , so when \mathbf{r} is inside S , and $r = |\mathbf{r}| < r_{\min}$, where r_{\min} is the radius of the sphere which inscribes S , the incident field is given by Eq. (4).

The scattered wave $\phi_s(\mathbf{r})$ is given for all $r=|\mathbf{r}| > r_{\max}$, i.e., for r outside a sphere of radius r_{\max} which circumscribes S . Therefore

$$\phi_s(\mathbf{r}) = \sum_n f_n \psi_n(\mathbf{r}) . \quad (5)$$

The reason is that all the sources giving rise to ϕ_s must lie completely inside the sphere on which the ψ_n (products with Hankel functions) are evaluated.

The field inside S is

$$\phi_t^-(\mathbf{r}) = \sum_n \alpha_n \text{Re} \psi'_n(\mathbf{r}) , \quad (6)$$

where “-” means “inside”, and the prime indicates acoustical conditions inside the scatterer.

There are two boundary equations which must be applied at the surface S . First, the continuity of pressure gives

$$\phi_t^+(\mathbf{r}') = \frac{\rho'}{\rho} \sum_n \alpha_n \text{Re} \psi'_n(\mathbf{r}') , \quad (7)$$

where ρ' indicates the density of the inner acoustic medium, and \mathbf{r}' is a point on S . Second, the continuity of the normal component of particle velocity gives

$$\nabla^+ \phi_t(\mathbf{r}') \cdot \mathbf{n} = \sum_n \alpha_n^e \nabla^- \text{Re} \psi'_n(\mathbf{r}') \cdot \mathbf{n} , \quad (8)$$

where \mathbf{n} is the normal to the surface.

Application of these relations to the EBC theorem leads to the following expression for the expansion coefficients appearing in Eq. (4) for the incident field, i.e.,

$$a_m = ik \iint_S \left\{ \psi_m(\mathbf{r}') \sum_n \alpha_n \nabla^- \text{Re} \psi'_n(\mathbf{r}') - \frac{\rho'}{\rho} \sum_n \alpha_n \text{Re} \psi'_n(\mathbf{r}') \nabla \psi_m(\mathbf{r}') \right\} \cdot \mathbf{n} dS . \quad (9)$$

This is an integral which must be performed over the surface area of the scatterer. Equation (9) represents a set of equations which can be written as a matrix equation

$$\mathbf{a} = -i\mathbf{Q}\bar{\alpha} , \quad (10)$$

where

$$Q_{mn} = k \iint_S \left\{ \frac{\rho'}{\rho} \text{Re} \psi'_n(\mathbf{r}') \nabla \psi_m(\mathbf{r}') - \psi_m(\mathbf{r}') \nabla^- \text{Re} \psi'_n(\mathbf{r}') \right\} \cdot \mathbf{n} dS . \quad (11)$$

Similar expressions are obtained for the expansion coefficients appearing in Eq. (5) for the incident field, i.e.,

$$f_m = -ik \iint_S \left\{ \text{Re} \psi_m(\mathbf{r}') \sum_n \alpha_n \nabla \text{Re} \psi'_n(\mathbf{r}') - \frac{\rho'^n}{\rho} \sum_n \alpha_n \text{Re} \psi'_n(\mathbf{r}') \nabla \text{Re} \psi_m(\mathbf{r}') \right\} \cdot \mathbf{n} dS \quad (12)$$

This leads to another set of equations which can be represented by

$$\mathbf{f} = i \text{Re} \mathbf{Q} \bar{\mathbf{a}} \quad , \quad (13)$$

where

$$\text{Re} Q_{mn} = k \iint_S \left\{ \frac{\rho'}{\rho} \text{Re} \psi'_n(\mathbf{r}') \nabla \text{Re} \psi_m(\mathbf{r}') - \text{Re} \psi_m(\mathbf{r}') \nabla \text{Re} \psi'_n(\mathbf{r}') \right\} \cdot \mathbf{n} dS \quad (14)$$

From Eq. (10) we have $\bar{\mathbf{a}} = i \mathbf{Q}^{-1} \mathbf{a}$, and substituting for $\bar{\mathbf{a}}$ in Eq. (13) yields

$$\mathbf{f} = -\text{Re} \mathbf{Q} \mathbf{Q}^{-1} \mathbf{a} = \mathbf{T} \mathbf{a} \quad \Rightarrow \quad \mathbf{T} \equiv -\text{Re} \mathbf{Q} \mathbf{Q}^{-1} \quad , \quad (15)$$

which is the general expression for the T-matrix \mathbf{T} .

2.2 Integration over the superspheroidal surface

For a superspheroid defined by: $(x/a)^s + (y/a)^s + (z/b)^s = 1$, the expression for the vector normal to the surface, after transformation to spherical coordinates and manipulation, may be shown to be

$$\hat{\mathbf{n}}(r, \theta, \phi) = \frac{\hat{r} (b^s \sin^s \theta + a^s \cos^s \theta) + \hat{\theta} (b^s \sin^{s-2} \theta - a^s \cos^{s-2} \theta) \sin \theta \cos \theta}{(b^{2s} \sin^{2s-2} \theta + a^{2s} \cos^{2s-2} \theta)^{1/2}} \quad , \quad (16)$$

which, we note, has no $\hat{\phi}$ dependence. This, when combined with the standard expression for ∇ in spherical coordinates, yields

$$\hat{\mathbf{n}}(r, \theta, \phi) \cdot \nabla \psi = \frac{(b^s \sin^s \theta + a^s \cos^s \theta) \frac{\partial \psi}{\partial r} + (b^s \sin^{s-2} \theta - a^s \cos^{s-2} \theta) \sin \theta \cos \theta \frac{1}{r} \frac{\partial \psi}{\partial \theta}}{(b^{2s} \sin^{2s-2} \theta + a^{2s} \cos^{2s-2} \theta)^{1/2}} \quad (17)$$

This indicates that, to determine the T-matrix elements for a superspheroidal scatterer, it is necessary to evaluate integrals of type $I = \int G(r, \theta) dS$ on the surface, where dS is

$$dS = \frac{a^2 b^2 (b^{2s} \sin^{2s-2} \theta + a^{2s} \cos^{2s-2} \theta)^{1/2}}{(b^s \sin^s \theta + a^s \cos^s \theta)^{(s+2)/s}} \sin \theta d\theta d\phi \quad , \quad (18)$$

and $r = b [(b/a)^s \sin^s \theta + \cos^s \theta]^{-1/s}$.

As an example, to show what these integrals typically look like, we have

$$Q_{n_1m,n_2m} = k \iint_S \left\{ \frac{\rho'}{\rho} j_{n_2}(k'r) Y_{n_2m} [C_1 k h'_{n_1}(kr) Y_{n_1m} + (C_2/r) h_{n_1}(kr) (\partial Y_{n_1m} / \partial \theta)] \right. \\ \left. - h_{n_1}(kr) Y_{n_1m} [C_1 k' j'_{n_2}(k'r) Y_{n_2m} + (C_2/r) j_{n_2}(k'r) (\partial Y_{n_2m} / \partial \theta)] \right\} dS, \quad (19)$$

which incorporates partial wave functions of the types $\psi_{nm}(k\mathbf{r}) = h_n(kr)Y_{nm}(\theta, \phi)$, and $\text{Re} \psi_{nm}(k'\mathbf{r}) = j_n(k'r)Y_{nm}(\theta, \phi)$ (where k' is the wavenumber inside the scatterer), and it is understood that $h'_n(kr) \equiv \partial h_n(kr) / \partial (kr)$, etc. The elements of $\text{Re} Q_{n_1m,n_2m}$ can be obtained in a corresponding manner, with $h_n \rightarrow j_n$ and $h'_n \rightarrow j'_n$. For a superspheroidal geometry, the structure of \mathbf{Q} (and also $\text{Re}\mathbf{Q}$) will be diagonal in m , but not generally diagonal in n .

3 Results

In the results below, we use the following equation to obtain the scattered acoustic wave field response in terms of standard angular distributions, and the elements of the T-matrix

$$F_\infty(k, \theta, \phi) = \frac{2}{ka} \left| \sum_{n,m} f_{nm} Y_{nm}(\theta, \phi) \right|, \quad (20)$$

where F_∞ denotes a “form function,” and a is radius of the spherical bubble of equivalent volume to the superspheroid.

One of the important features of Eq. (15) to find the f_{nm} , and therefore the scattered field, is that \mathbf{T} is a function only of the boundary conditions and the shape of the object. Consequently, once \mathbf{T} is known, the scattered field can be determined from any chosen incident field. However, a straightforward evaluation of Eq. (15) is frequently problematical. The reason is that \mathbf{Q} is typically very large, and often ill-conditioned, so that finding \mathbf{Q}^{-1} is difficult. Various computational strategies have been adopted to deal with this issue. In this present work, the computational scheme was implemented using *MATLAB*. In addition, use was made of a freely downloadable software package “mptoolbox_1.1” (Barrowes, 2007) which enables numerical computations to be performed to arbitrary degrees of precision. For the work here, this toolbox was implemented with 250 bits of precision specified for the mantissa part of the number, which leads to computations with about 75 decimal places of accuracy. This is easily enough to determine \mathbf{Q}^{-1} for all the cases considered here.

In the calculations here, the density and sound speed of water are taken as $\rho = 1000 \text{ Kg/m}^3$ and $c = 1500 \text{ m/s}$, respectively. The density and sound speed of air are $\rho' = 1.26 \text{ Kg/m}^3$ and $c' = 331.5 \text{ m/s}$, respectively.

3.1 The shape of superspheroids

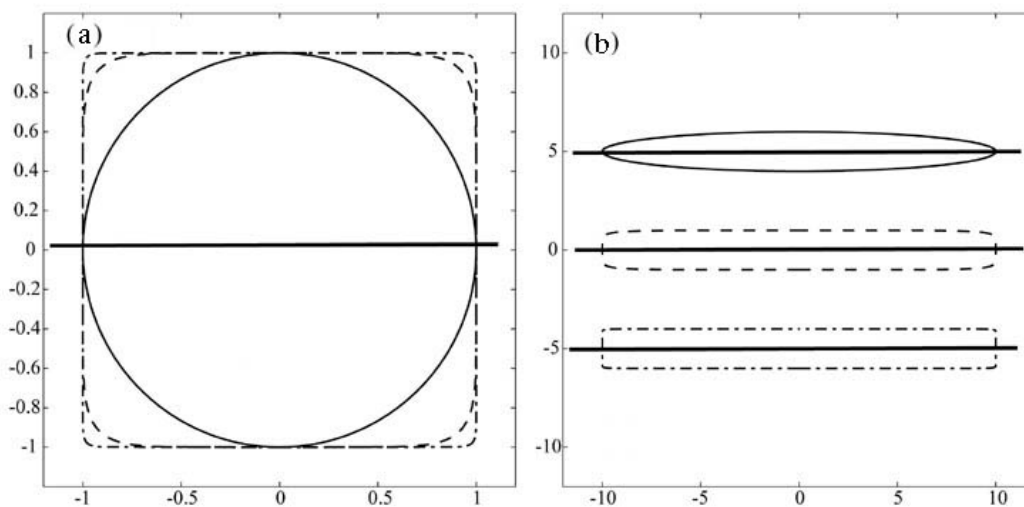


Figure 1. Change of shape of superspheroids. (a) $\alpha=1$. (b) $\alpha=10$. In both cases: $s = 2$ (solid line); $s = 8$ (dashed line); $s = 32$ (dot-dash line). The heavy horizontal lines show the axis around which the curve must be rotated to form a 3-D object. (Curves vertically separated for $\alpha=10$, for clarity).

Figure 1 shows the effect of increasing the superspheroid order on the shape of scattering object. When $s=32$, the shape approximates closely to a right circular cylinder.

3.2 The effect of increasing aspect ratio

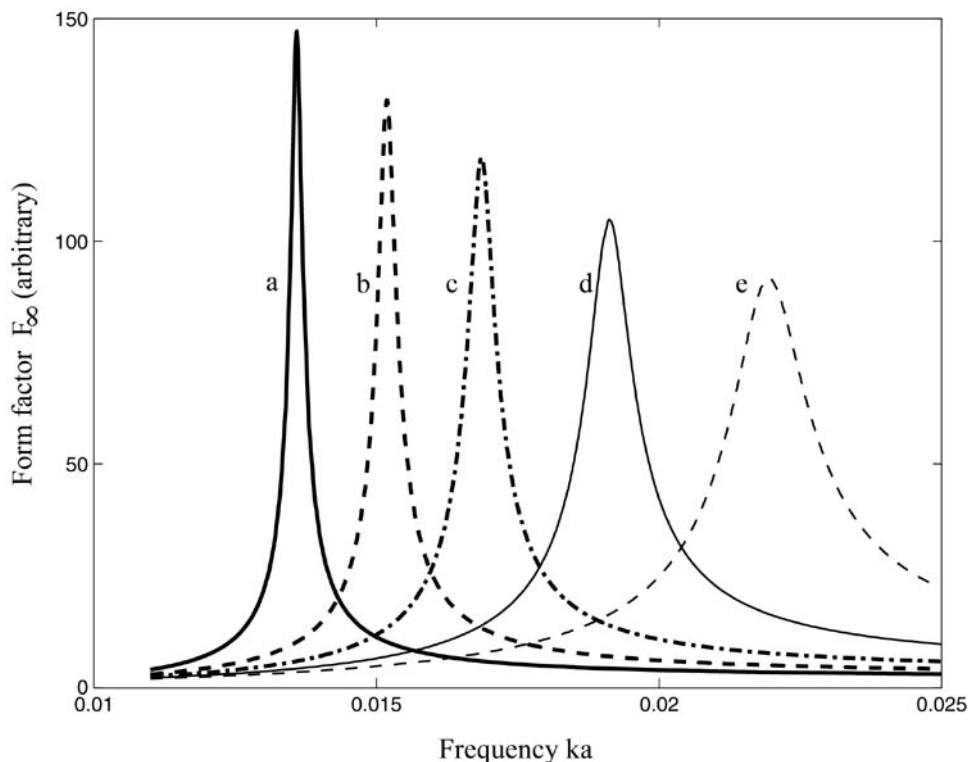


Figure 2. Change of form function with aspect ratio. (a) $\alpha=1$. (b) $\alpha=5$. (c) $\alpha=10$. (d) $\alpha=20$. (e) $\alpha=40$. In all cases $s = 2$.

Figure 2 shows the effect of varying the aspect ratio α on the primary low frequency resonance of superspheroids of order $s = 2$ (i.e., they are pure prolate spheroids). The form function is plotted as a function of frequency represented by ka . In all cases, the scatterers were insonified from broadside ($\theta = 90^\circ$). Based on the form function, three effects may be observed: (1) the resonance frequency ka_α increases; (2) the maximum peak height P_{\max} decreases; (3) the quality-factor Q_f of the resonance (determined by dividing ka_α by the 3-dB width of the response) decreases. These effects are summarised in Table 1.

Table 1. Effect of changing aspect ratio on resonance properties

Aspect ratio α	ka_α	ka_α / ka_1	P_{\max}	Q_f
1	0.01359	1	147.09	75
5	0.01520	1.1185	130.91	50
10	0.01686	1.2406	118.70	37
20	0.01902	1.3996	114.81	27
40	0.02190	1.6115	91.56	18

The values of Q_f presented here tend to vary with the specific sampling interval used to calculate the curves and, consequently, can only claim an accuracy of about ± 1 in the last integer before the decimal point. The ratio ka_α / ka_1 closely matches the values predicted by Weston's formula for the resonance frequency of a prolate spheroid.⁵

$$\frac{f_e}{f_1} = \sqrt{2} e^{-1/3} (1-e^2)^{1/4} \left\{ \log_e \left[\frac{1+(1-e^2)^{1/2}}{1-(1-e^2)^{1/2}} \right] \right\}^{-1/2}, \quad (21)$$

where $e = \alpha^{-1}$.

3.3 The effect of increasing superspheroid order, and azimuthal variations

Figure 3 shows the effect of increasing the superspheroid order on the characteristics of the resonance. As when the aspect ratio was varied, increasing s has three effects: (1) ka_α increases; (2) P_{\max} decreases; (3) Q_f decreases. However, these effects are now much smaller than when the aspect ratio was increased. The effects are summarised in Table 2.

Table 2. Effect of increasing s on resonance properties

Aspect ratio α	Order s	ka_α	ka_α / ka_1	P_{\max}	Q_f
1	2	0.01359	1	147.09	75
1	8	0.01373	1.0103	145.61	72
1	32	0.01379	1.0147	145.01	73
10	2	0.01686	1	118.70	37
10	8	0.01718	1.0189	116.47	36
10	32	0.01730	1.0261	115.65	36

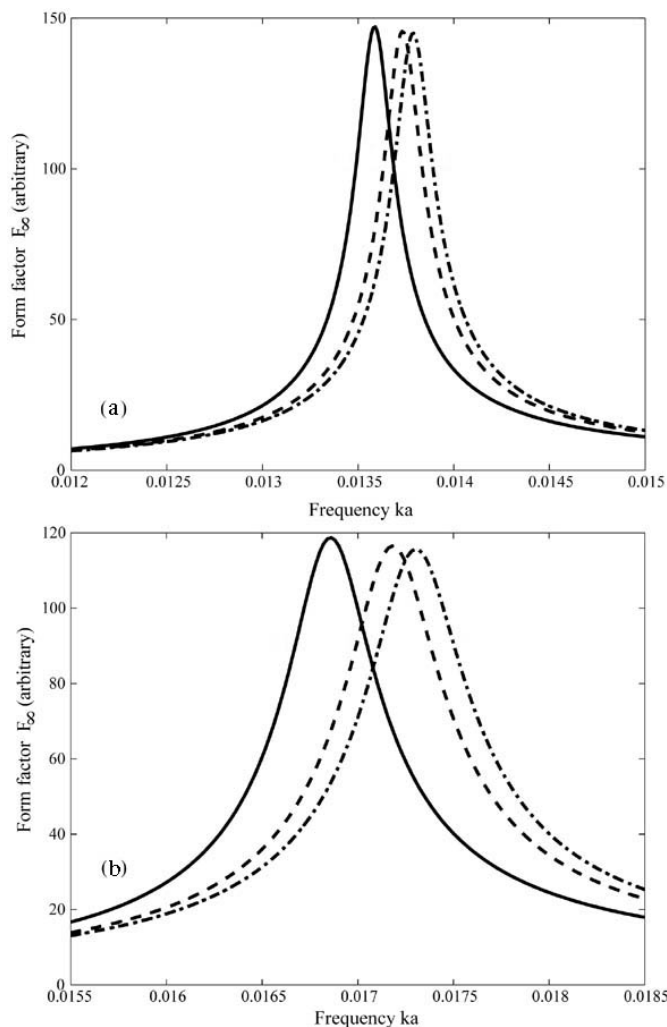


Figure 3. Variations in resonance peak with s . (a) $\alpha=1$. (b) $\alpha=10$. In both cases: $s = 2$ (solid line); $s = 8$ (dashed line); $s = 32$ (dot-dash line).

A value $\alpha=10$ (rather than greater) was chosen here because this is an aspect ratio more typical for fish swimbladders. Figure 1 shows that when $s=32$, the shape of the scatterer already approximates closely to a right circular cylinder. Further computations (not shown) indicate that higher values of s do not lead to significant changes in ka_α , P_{max} , and Q_f .

Table 3 shows values of the broadside to endfire scattered field ratio for both monostatic and bistatic (incident angles $\theta_i = 0^\circ$ and $\theta_i = 90^\circ$) geometries.

Table 3. Ratios of broadside to endfire scattering amplitude

α	s	Ratio (mono)	Ratio (bi : $\theta_i = 0^\circ$)	Ratio (bi : $\theta_i = 90^\circ$)
1	2	1	1	1
10	2	1.0021	1.0010	1.0010
40	2	1.0212	1.0104	1.0102
1	32	1.0000	1.0000	1.0000
10	32	1.0025	1.0012	1.0012
40	32	1.0240	1.0113	1.0113

The objects were insonified at the appropriate resonance frequency, as indicated in Tables 1 and 2, for each combination of α and s . Even for values as high as $\alpha=40$ and $s=32$, the azimuthal distribution of the scattered field is essentially spherically symmetric. Table 3 shows that the field deviates from spherical symmetry by less than 3% for either monostatic or bistatic scattering schemes.

The results presented in this work support the assumption that the effect of introducing irregularities onto the surfaces of bubbles and swimbladders, insonified at low frequency, is generally negligible. The monopole resonance, which leads to a spherically symmetric scattering distribution, continues to dominate low frequency scattering even for cylindrically shaped, air-filled, objects with an aspect ratio up to $\alpha=40$. The use of spherical scatterer models to describe low frequency scattering from fish swimbladders appears to be well justified.

References

- Tate, John T (1969). "Physics of Sound in the Sea". U.S. Government Printing Office, Washington DC, USA.
- Minnaert, M (1933). "On musical air-bubbles and the sounds of running water". *Philosophical Magazine*, (16), 235-248.
- Anderson, V C (1950), "Sound scattering from a fluid sphere" *Journal of the Acoustical Society of America*, (22), 426-431.
- Strasberg, M (1953). "The pulsation frequency of nonspherical gas bubbles in liquids," *Journal of the Acoustical Society of America*, (25), 536-537.
- Weston, D E (1967). "Sound propagation in the presence of bladder fish". in "Underwater Acoustics". Plenum, New York, USA.
- Ye, Z 1(998). "Low frequency acoustic scattering by gas-filled prolate spheroids. II. Comparison with exact solution". *Journal of the Acoustical Society of America*, (103) 2, 822-826.
- Feuillade, C; Werby, M W (1994). " Resonances of deformed gas bubbles in liquid". *Journal of the Acoustical Society of America*, (96) 6, 536-537.
- Waterman, P C (1969). "New formulation of acoustic scattering". *Journal of the Acoustical Society of America*, (45) , 1417-1429. T.K. Stanton, "Sound scattering by cylinders of finite length. I. Fluid cylinders," *J. Acoust. Soc. Am.*, **83**, 55-63 (1988).
- Stanton, T K (1988). "Sound scattering by cylinders of finite length. I. Fluid cylinders". *Journal of the Acoustical Society of America*, (83) , 55-63.
- Stanton, T K (1989). "Sound scattering by cylinders of finite length. III. Deformed cylinders". *Journal of the Acoustical Society of America*, (86) , 691-705.
- Barrowes, Ben (2007) "<http://webscripts.softpedia.com/script/Scientific-Engineering-Ruby/Mathematics/Multiple-Precision-Toolbox-for-MATLAB-34002.html>"